Journal of Power Sources 259 (2014) 188–194

Contents lists available at ScienceDirect

Journal of Power Sources

journal homepage: www.elsevier.com/locate/jpowsour

Enhanced electrochemical performances of $LiNi_{0.5}Mn_{1.5}O_4$ by surface modification with superconducting $YBa_2Cu_3O_7$

Yingbin Lin [a,b,*], Yanmin Yang [a], Ruibing Yu [a], Heng Lai [a], Zhigao Huang [a,b]

[a] College of Physics and Energy, Fujian Normal University, Fuzhou 350108, China
[b] Fujian Provincial Key Laboratory of Quantum Manipulation and New Energy Materials, Fujian Normal University, Fuzhou 350108, China

HIGHLIGHTS

- $YBa_2Cu_3O_7$-coating enhances the rate capability and cyclability of $LiNi_{0.5}Mn_{1.5}O_4$.
- Superconducting $YBa_2Cu_3O_7$ reduces charge-transfer resistance in a wide temperature.
- $YBa_2Cu_3O_7$ facilitates the kinetics for lithium diffusion at low temperature.

ARTICLE INFO

Article history:
Received 17 December 2013
Received in revised form
1 February 2014
Accepted 23 February 2014
Available online 6 March 2014

Keywords:
Lithium-ion batteries
Lithium nickel manganese oxide
Superconductor
Surface modification

ABSTRACT

$LiNi_{0.5}Mn_{1.5}O_4$ modified with superconducting $YBa_2Cu_3O_7$ (YBCO) is synthesized by mixing as-prepared $LiNi_{0.5}Mn_{1.5}O_4$ powders and the sol–gel-driven $YBa_2Cu_3O_7$ matrix, subsequently followed by high-temperature calcinations. The effect of YBCO-modification on the electrochemical performances of $LiNi_{0.5}Mn_{1.5}O_4$@YBCO cells in a wide operation temperature is investigated systematically by the charge/discharge testing, cyclic voltammograms and AC impedance spectroscopy, respectively. In comparison with the pristine $LiNi_{0.5}Mn_{1.5}O_4$, $LiNi_{0.5}Mn_{1.5}O_4$@YBCO samples exhibit higher capacity, better cyclability and higher rate capability in a wide operation temperature range. An analysis of the electrochemical measurements reveals that the improved performance of $LiNi_{0.5}Mn_{1.5}O_4$@YBCO is due to the better electric contact among particles, much lower charge-transfer resistances and higher lithium diffusion rate, especially at low temperature. In addition, the homogeneous YBCO layer formed on the $LiNi_{0.5}Mn_{1.5}O_4$ protects the active materials from chemical attack by HF, which suppresses the dissolution of Ni or Mn from $LiNi_{0.5}Mn_{1.5}O_4$ in the $LiPF_6$ based electrolyte.

1. Introduction

Recently, great interest has arisen in application of high voltage spinel cathode material for lithium-ion secondary batteries due to its high discharge capacity and attractive voltage plateau at around 4.7 V, which offers its potential application in electric vehicle and plug-in hybrid electric vehicle [1–3]. Although considerable progress has been made in spinel cathodes as far [4–7], serious issues regarding the capacity fading and poor rate performances make them less favorable for practical application, which might result from the decomposition of the electrolyte at high operating voltage or Mn dissolution caused by HF in the electrolyte, especially at elevated temperature [8,9]. Tremendous efforts have been devoted to the improvement of the cyclic stability for spinel cathode by surface modification with metal oxide [8–12], such as SiO_2, ZrO_2, $LiFePO_4$, $AlPO_4$ and $LiAlO_2$. For instance, Wu et al. [8] have reported that the $LiNi_{0.5}Mn_{1.5}O_4$ modified by ZrO_2 exhibits significantly enhanced electrochemical reversibility at elevated temperature. Liu et al. [9] have revealed that the surface modification of $LiNi_{0.5}Mn_{1.5}O_4$ with C-$LiFePO_4$ shows enhanced rate capability and improved capacity retention rate. However, it is well-known that most metal oxide demonstrates high resistivity due to its insulating or semi-conducting behavior in terms of the electrical conductivity, resulting in large polarization of the electrode and consequently hampering Li-ion battery application at low operation temperature. In contrast, superconducting $YBa_2Cu_3O_7$ demonstrates a stable low-resistivity state in a wide temperature range and its resistivity decreases with decreasing temperature which is similar to that of

* Corresponding author. College of Physics and Energy, Fujian Normal University, Fuzhou 350108, China. Tel./fax: +86 591 2286 8132.
E-mail addresses: yblin@fjnu.edu.cn, linyingbin@gmail.com (Y. Lin), zghuang@fjnu.edu.cn (Z. Huang).

http://dx.doi.org/10.1016/j.jpowsour.2014.02.093
0378-7753/

the metal [13]. Therefore, $LiNi_{0.5}Mn_{1.5}O_4$@YBCO composite would be highly desirable for the application of Li-ion batteries in wide-range temperature, where the formation of YBCO integrate network in composite not only provides a high conductive nano-layer between particles but also protects the active materials from chemical attack by HF in electrolyte. In present work, the surface modification of $LiNi_{0.5}Mn_{1.5}O_4$ with YBCO was synthesized by a simple sol–gel method. Compared to the pristine $LiNi_{0.5}Mn_{1.5}O_4$, the as-prepared $LiNi_{0.5}Mn_{1.5}O_4$@YBCO exhibits superior electrochemical performances in a wide operation temperature range.

2. Experimental

2.1. Preparation and characterization of cathode materials

$LiNi_{0.5}Mn_{1.5}O_4$ and $LiNi_{0.5}Mn_{1.5}O_4$@YBCO composites were fabricated by a simple sol–gel method. In detail, analytical grade $LiCH_3COO\cdot 2H_2O$, $Mn(CH_3COO)_2\cdot 6H_2O$, and $Ni(CH_3COO)_2\cdot 4H_2O$ in stoichiometric amounts were thoroughly dissolved in de-ionized water containing proper amount of citric acid solution followed by stirring at 80 °C until the polymerized gel was formed. The obtained gel is dried at 120 °C to form amorphous powders. The powder was further sintered at 500 °C for 12 h to complete organic removal and subsequently calcined at 850 °C for 20 h to obtain $LiNi_{0.5}Mn_{1.5}O_4$ powder. $(LiNi_{0.5}Mn_{1.5}O_4)_{95}$@$(YBCO)_5$ (denoted as $(LNMO)_{95}$@$(YBCO)_5$)cathode material was synthesized by mixing appropriate amounts of as-prepared $LiNi_{0.5}Mn_{1.5}O_4$ powder with $YBa_2Cu_3O_7$ gel under ultrasonic-treatment, where the preparation of $YBa_2Cu_3O_7$ gel was described in detail in Kakihana's work [14]. The resulted gel is dried at 120 °C in atmosphere, followed by calcinations at 900 °C for 10 h to obtain the final products. In comparison, the pristine $YBa_2Cu_3O_7$ was prepared under the same preparation condition. The phase indentification of the pristine $LiNi_{0.5}Mn_{1.5}O_4$ and $(LNMO)_{95}$@$(YBCO)_5$ powders was conducted with an X-ray diffractometer (XRD, Rigaku MiniFlex II) using CuK_α radiation ($\lambda = 0.15405$ nm). The morphology of the composites was studied with a scanning electron microscope (SEM, JSM-7500F, Japan). The nanoscale microstructure of $(LNMO)_{95}$@$(YBCO)_5$ particles was examined using a transmission electron microscope (TEM, Tecnai G2 F20 S-TWIN). Electrical properties were measured by a Versalab magnetometer (Versalab, Quantum Design Co.).

2.2. Cell fabrication and characterization

The working electrode was prepared by homogeneously pasting a slurry containing 80 wt.% active material ($LiNi_{0.5}Mn_{1.5}O_4$ or $(LNMO)_{95}$@$(YBCO)_5$), 10 wt.% super-P and 10 wt.% polyvinylidene fluoride (PVDF) dissolved in N-methyl-2-pyrrolidone on an Al foil and subsequently dried in vacuum at 110 °C over night. The coin cells (R2025) were assembled in an argon-filled glove box (Mikrouna, Super 1220/750, China) with Li metal as anode and counter electrode, Celgard 2300 microporous polyethylene membrane as separator and 1M $LiPF_6$ in a mixture of ethyl carbonate (EC) and dimethyl carbonate (DMC) (1:1 in vol. ratio) as electrolyte. Galvanostatic charge/discharge measurements were carried out in the voltage range of 3.0–4.9 V with a CT2001A cell test instrument (LAND Electronic Co.). Cyclic voltammograms (CV) and electrochemical impedance spectra (EIS) measurements were performed by electrochemical workstation (CHI660C) in a frequency range from 10 mHz to 100 KHz with an amplitude of 5 mV.

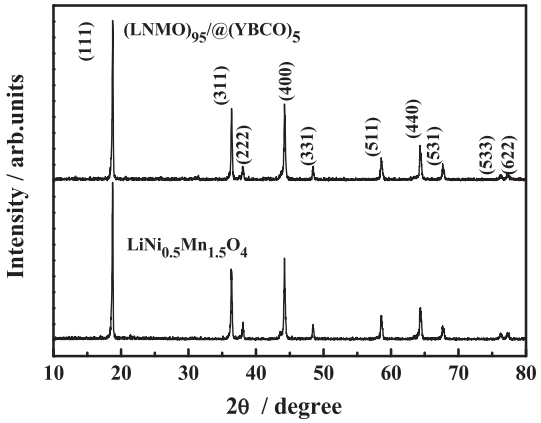

Fig. 1. XRD patterns of $LiNi_{0.5}Mn_{1.5}O_4$ and $(LNMO)_{95}$@$(YBCO)_5$ powders.

3. Results and discussion

3.1. Material characterization

Fig. 1 shows XRD patterns of the pristine and $(LNMO)_{95}$@$(YBCO)_5$ powders. All the observed diffraction peaks for both samples can be indexed well based on a cubic spinel structure with Fd-3m space group (ICSD#070046), in which Li^+ ions occupy the tetrahedral (8a) sites and the transition metal ions (Ni and Mn) statistically reside at the octahedral (16d) site. Besides the main $LiNi_{0.5}Mn_{1.5}O_4$ spinel phase, no diffraction pattern corresponding to the coating material is found within the sensitivity of measurement since the amount of coating material is small (about 5.0 wt.%).

Fig. 2(a) and (b) shows the surface morphologies examined by SEM for the pristine and $(LNMO)_{95}$@$(YBCO)_5$ composites, respectively. It is clear that the pristine $LiNi_{0.5}Mn_{1.5}O_4$ particles exhibit smooth and clean surface morphology with sharp edges, while the surface of $(LNMO)_{95}$@$(YBCO)_5$ is covered uniformly with small particles, shown in Fig. 2(b). Fig. 3 shows TEM image of $(LNMO)_{95}$@$(YBCO)_5$, which further confirms the existence of YBCO particles and YBCO-coating layer on the surface of $LiNi_{0.5}Mn_{1.5}O_4$. The YBCO-coating layer has a thickness of approximately 50 nm.

Fig. 4 shows the temperature (T) dependence of resistivity (ρ) of YBCO composite synthesized as same as that of YBCO in $(LNMO)_{95}$@$(YBCO)_5$ composite, which is measured by a typical four-probe method. The electrical resistivity of as-prepared YBCO drops with a jump down to zero around ~80 K, which is the typical characteristic of superconductivity [15]. The obtained results indicate that small particles on LiNi0.5Mn1.5O4 consist mainly of superconducting YBCO. Such homogeneous YBCO-coating is expected to form high conducting network between particles and efficiently prevents the transition metal ions dissolution from spinel cathode, resulting in a superior discharge/charge performance especially at low temperature.

Fig. 5(a) presents the discharge capacities vs. cycle number of the pristine and $(LNMO)_{95}$@$(YBCO)_5$ cathodes at 0.5, 1, 2, 4, 5 and 6C rate (1C = 148 mAh g^{-1}) between 3.0 and 4.9 V at 20 °C. With the surface modification of YBCO layer, $(LNMO)_{95}$@$(YBCO)_5$ exhibits higher capacity (0.5C: 122 mA h g^{-1}; 1C: 119.8 mAh g^{-1}; 2C: 116.7 mAh g^{-1}; 4C: 112.8 mAh g^{-1}, 5C: 110.7 mAh g^{-1}, 6C: 108.9 mAh g^{-1}, respectively) than that of $LiNi_{0.5}Mn_{1.5}O_4$ (0.5C: 122.5 mAh g^{-1}; 1C: 117.7 mAh g^{-1}; 2C: 111.6 mAh g^{-1}; 4C: 105.5 mAh g^{-1}, 5C: 101.4 mAh g^{-1}, 6C: 97.2 mAh g^{-1}, respectively), especially at high rate. Moreover, $(LNMO)_{95}$@$(YBCO)_5$ also demonstrates superior high-rate performance and capacity cyclability when cycled under very high rate of 10C and 20C for 100 times respectively, shown in Fig. 5(b).

To further understand the improved rate performance of YBCO-surface modified composite, Fig. 6(a) and (b) compares the charge and discharge curve of the pristine and $(LNMO)_{95}$@$(YBCO)_5$ as a

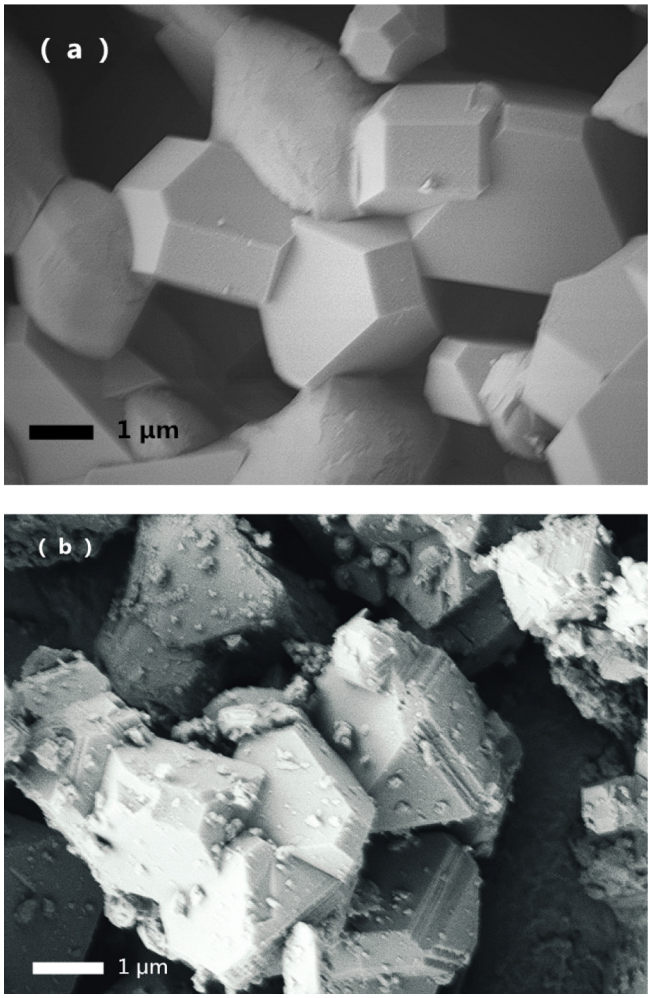

Fig. 2. SEM images of (a) $LiNi_{0.5}Mn_{1.5}O_4$ and (b) $(LNMO)_{95}@(YBCO)_5$ powders.

function of the cycle number with C rates increasing from 0.5C to 6C, respectively. It is found that the charge curves of both samples shift toward higher potential while the discharge curves move to lower potential when the current density increases. Such polarization behavior is much more obvious in the corresponding differential capacity, shown in Fig. 6(c) and (d). It is clear that the reduction peaks move to lower potential with increasing current density while the oxidation peaks move toward higher potential, resulting in the larger separation between the oxidation and reduction peaks. In addition, the peak separation of $(LNMO)_{95}@(YBCO)_5$ is smaller than that of the pristine one at the same current density. Moreover, in comparison with $LiNi_{0.5}Mn_{1.5}O_4$, the separation between two reduction (or oxidation) peaks in the dQ/dV curves of $(LNMO)_{95}@(YBCO)_5$ are still clearly observed even under a high current density of 6C, which indicates that the YBCO-coating could significantly reduces the polarization and consequently enhances the high-rate capacity cyclability [16].

Fig. 7 shows the capacity cyclability of cells based on lithium metals as the anode and the $LiNi_{0.5}Mn_{1.5}O_4$ and $(LNMO)_{95}@(YBCO)_5$ as the cathode, which was carried out at 2.0C and 60 °C for 100 cycles. Comparing to the electrochemical performances at 20 °C, higher capacities are obtained at 60 °C due to the improved kinetics of lithium diffusion because Li-ion transfer activity is accelerated between the anode and cathode at the elevated temperature [17]. Comparing to the pristine $LiNi_{0.5}Mn_{1.5}O_4$, $(LNMO)_{95}@(YBCO)_5$ obviously demonstrates superior capacity cyclability. The initial

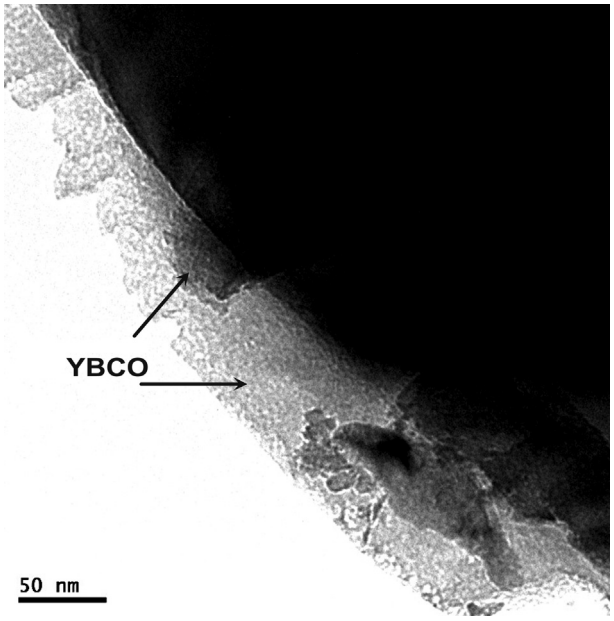

Fig. 3. TEM image of $(LNMO)_{95}@(YBCO)_5$.

discharge capacity of $(LNMO)_{95}@(YBCO)_5$ is 128.6 mA h g^{-1} and it is found to decay gradually with continuous cycling, retaining 112 mA h g^{-1} after 100 cycles. The $LiNi_{0.5}Mn_{1.5}O_4$ exhibits initial capacity of 130.8 mA h g^{-1} and but its capacity fade faster to 90.5 mA h g^{-1} in totally 100 cycles, suffering a more than 30% capacity loss. It is well-established that the high surface reactivity of the Ni^{4+} from charged $LiNi_{0.5}Mn_{1.5}O_4$ with $LiPF_6$-based non-aqueous electrolyte should be responsible for the poor cycling performance, especially at the elevated temperature [8]. The YBCO layer on the $LiNi_{0.5}Mn_{1.5}O_4$ surface is expected to efficiently suppress the surface reactivity between the charged electrode and the electrolyte during electrochemical cycling. As a result, the electrochemical reversibility is correspondingly improved.

To better understand the superior cycling stability of $(LNMO)_{95}@(YBCO)_5$ at the elevated temperature, AC impendence studies of the cells after 100 cycles at 2.0C and 60 °C were carried out. Fig. 8 presents EIS profiles of the $LiNi_{0.5}Mn_{1.5}O_4$ and $(LNMO)_{95}@(YBCO)_5$ and the corresponding equivalent circuit. According to the literature [6], the symbols, R_e, R_{sf}, R_{ct}, and R_w, represent the solution resistance, the diffusion resistance of Li^+ ions through SEI layer, the charge transfer resistance and Warburg

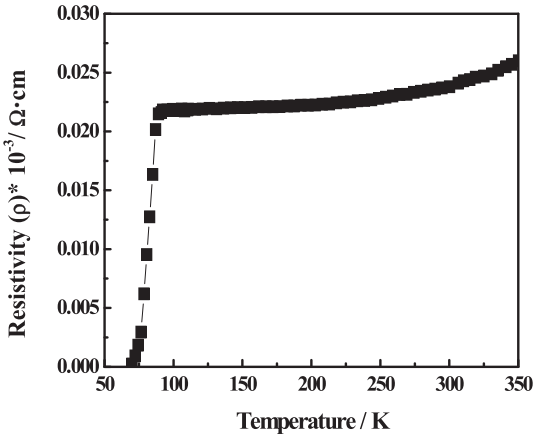

Fig. 4. Temperature (T) dependence of resistivity (ρ) of YBCO composite.

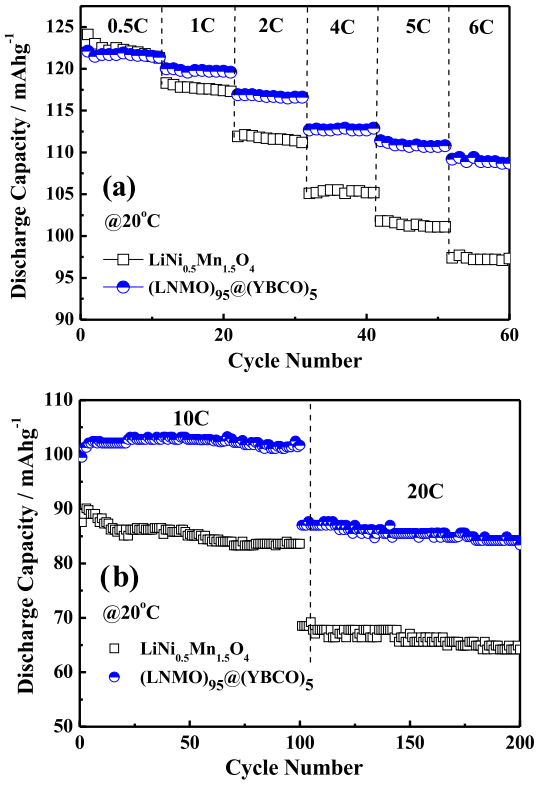

Fig. 5. (a) Rate capability of $LiNi_{0.5}Mn_{1.5}O_4$ and $(LNMO)_{95}@(YBCO)_5$; (b) Cycling performances of $LiNi_{0.5}Mn_{1.5}O_4$ and $(LNMO)_{95}@(YBCO)_5$ at 10C and 20C.

impedance related to the solid-state diffusion of Li^+ in the active materials, respectively. According to the equivalent circuit, individual contribution from each of solution resistance, diffusion resistance and charge-transfer resistance are calculated as 6.50 Ω, 256.1 Ω and 73.47 Ω for LiNi0.5Mn1.5O4 and 7.11 Ω, 34.67 Ω and 18.11 Ω for $(LNMO)_{95}@(YBCO)_5$, respectively. It is found that $LiNi_{0.5}Mn_{1.5}O_4$ has larger charge-transfer resistance (R_{ct}) than that of $(LNMO)_{95}@(YBCO)_5$ due to the formation of SEI layer (RCH_2O-CO_2Li, LiF, MnF_2, Li_2CO_3 and so on) on the cathode surface, resulting from the oxidized and decomposition of the electrolyte [18,19]. The formation of SEI layer is responsible for slowing down of the kinetics of these electrodes through the obstruction of the pore upon cycling [20] and high-conductivity YBCO on the surface is expected to overcome the kinetics restrictions during the charge/discharge process [21,22].

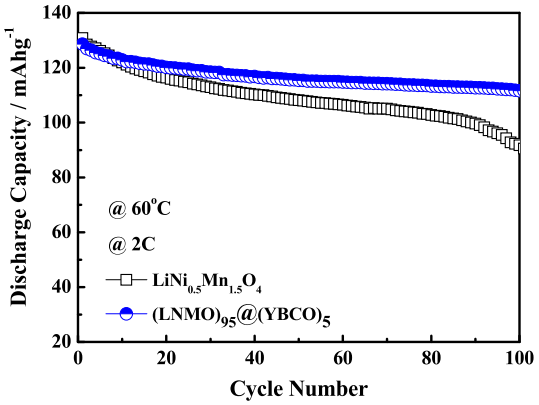

Fig. 7. Cycling performances of $LiNi_{0.5}Mn_{1.5}O_4$ and $(LNMO)_{95}@(YBCO)_5$ at 2.0C and 60 °C.

Good low-temperature performance is highly desirable for specific applications of Li-ion batteries. Fig. 9 presents the specific capacities as a function of cycle number for $LiNi_{0.5}Mn_{1.5}O_4$ and $(LNMO)_{95}@(YBCO)_5$ at different temperature (0, −10, −20 and −30 °C) and 2C rate in the voltage range of 3.0–5.0 V. In contrast, the beneficial effect of YBCO-coating in reducing capacity fading of $LiNi_{0.5}Mn_{1.5}O_4$ at low temperature is obviously observed.

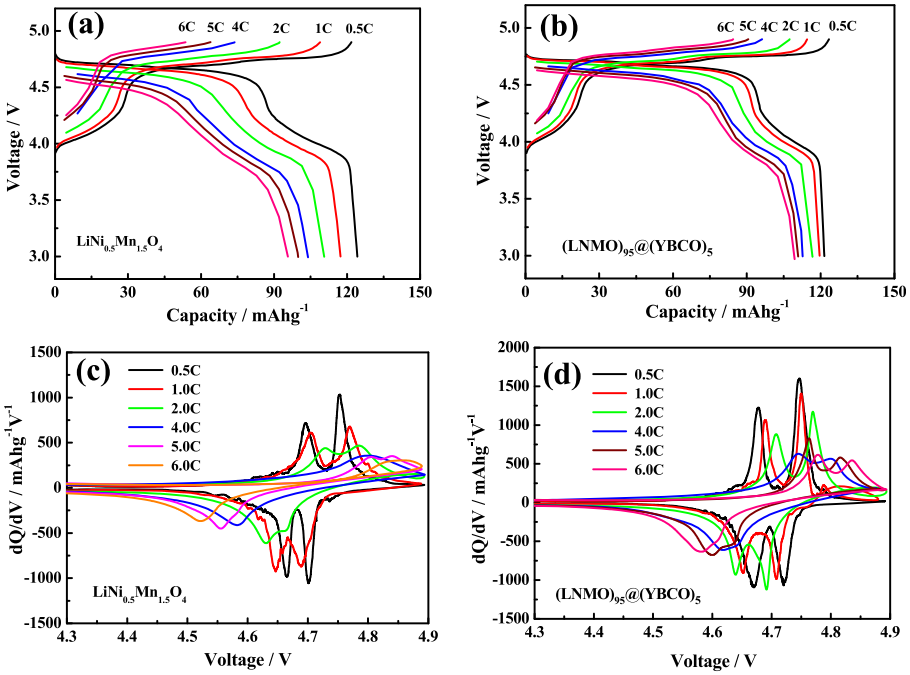

Fig. 6. Charge-discharge profiles of (a) $LiNi_{0.5}Mn_{1.5}O_4$ and (b) $(LNMO)_{95}@(YBCO)_5$ at various rate; Differential capacity of (c) $LiNi_{0.5}Mn_{1.5}O_4$ and (d) $(LNMO)_{95}@(YBCO)_5$ with C rates increasing from 0.5C to 6C.

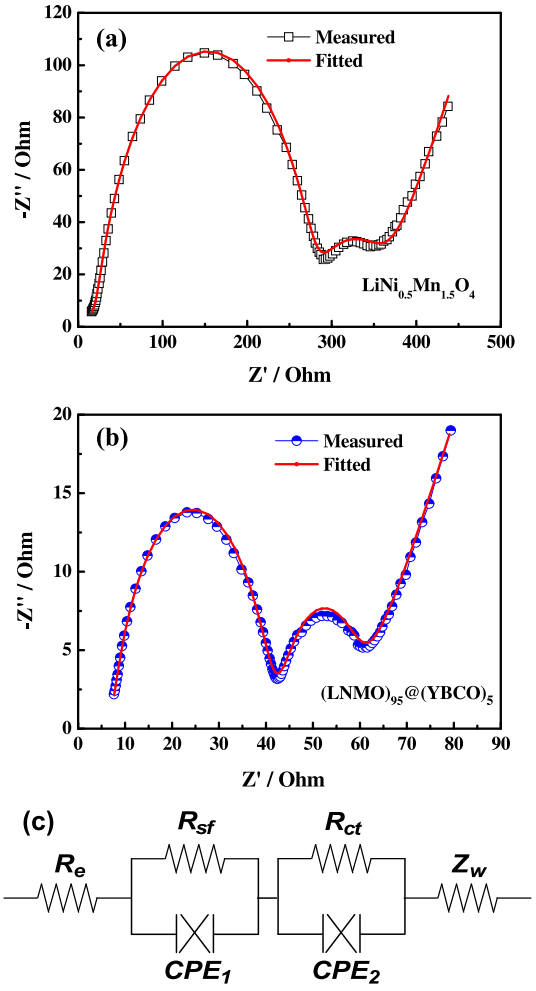

Fig. 8. The EIS profiles of (a) $LiNi_{0.5}Mn_{1.5}O_4$ and (b) $(LNMO)_{95}@(YBCO)_5$ after 100 cycles at 2C rate and 60 °C; (b) the equivalent circuit for EIS results fitting.

$(LNMO)_{95}@(YBCO)_5$ as a whole exhibits higher capacity (0 °C: 105 mA h g^{-1}; −10 °C: 95 mA h g^{-1}; −20 °C: 77 mA h g^{-1}; −30 °C: 54 mA h g^{-1}, respectively) than the pristine $LiNi_{0.5}Mn_{1.5}O_4$ (0 °C: 101 mA h g^{-1}; −10 °C: 79 mA h g^{-1}; −20 °C: 51 mA h g^{-1}; −30 °C: 24 mA h g^{-1}, respectively), which might be associated with the excellent conductivity of YBCO in all temperature range, especially at low temperature.

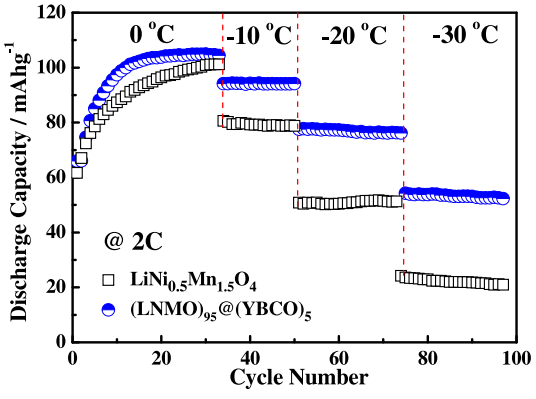

Fig. 9. Rate capability of $LiNi_{0.5}Mn_{1.5}O_4$ and $(LNMO)_{95}@(YBCO)_5$ at different temperature (0, −10, −20 and −30 °C) and 2C rate.

As far as the superior performances of $(LiNi_{0.5}Mn_{1.5}O_4)_{95}@(YBCO)_5$ at low temperature is concerned, further investigation on lithium diffusive properties were carried out using the electrochemical impedance spectroscopy (EIS) from 0 °C to −30 °C, shown in Fig. 10. It is found that the impedance spectrum is composed of two partially overlapped semicircles at

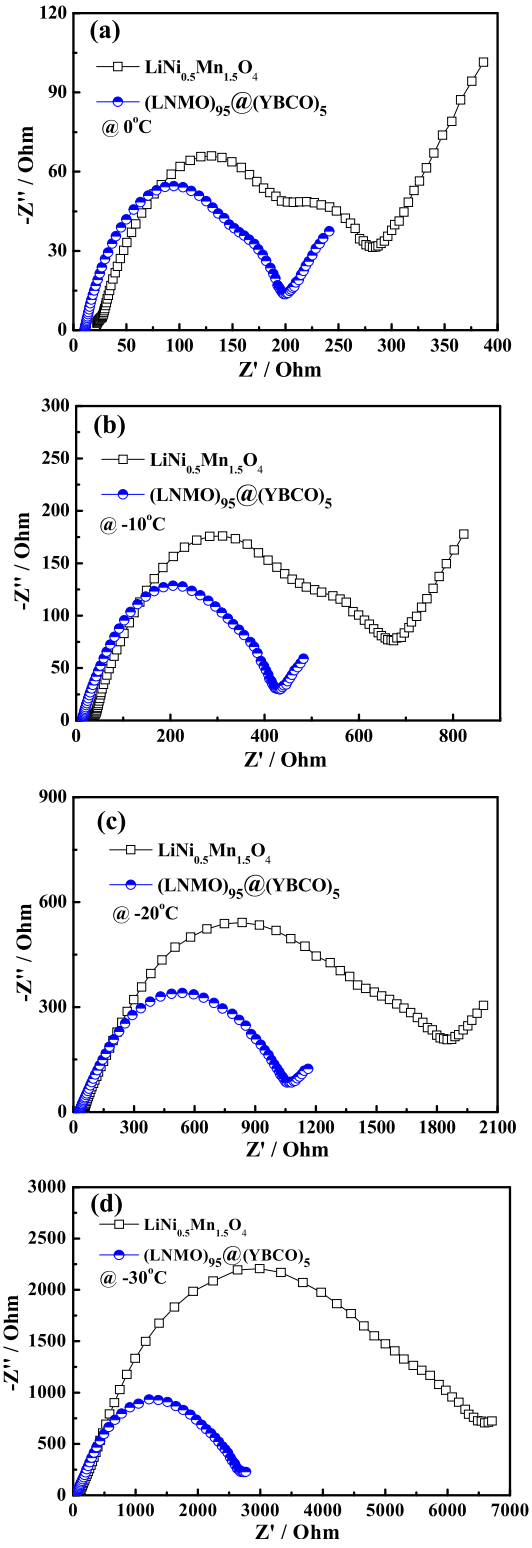

Fig. 10. EIS for $LiNi_{0.5}Mn_{1.5}O_4$ and $(LNMO)_{95}@(YBCO)_5$ at different temperature.

high and medium frequencies, and an oblique straight line at low frequencies. In addition, two semicircles overlap more distinctly with the decreasing temperature and become a non-resolved semicircle, which reflects the interface impedance including both R_{SEI} and R_{ct} [23]. Moreover, the interface impedance (R_{SEI} + R_{ct}) of $(LNMO)_{95}$@$(YBCO)_5$ is much smaller than that of the pristine one especially at low temperature, resulting from the suppressed development of SEI layer and relatively faster ionic migration [24].

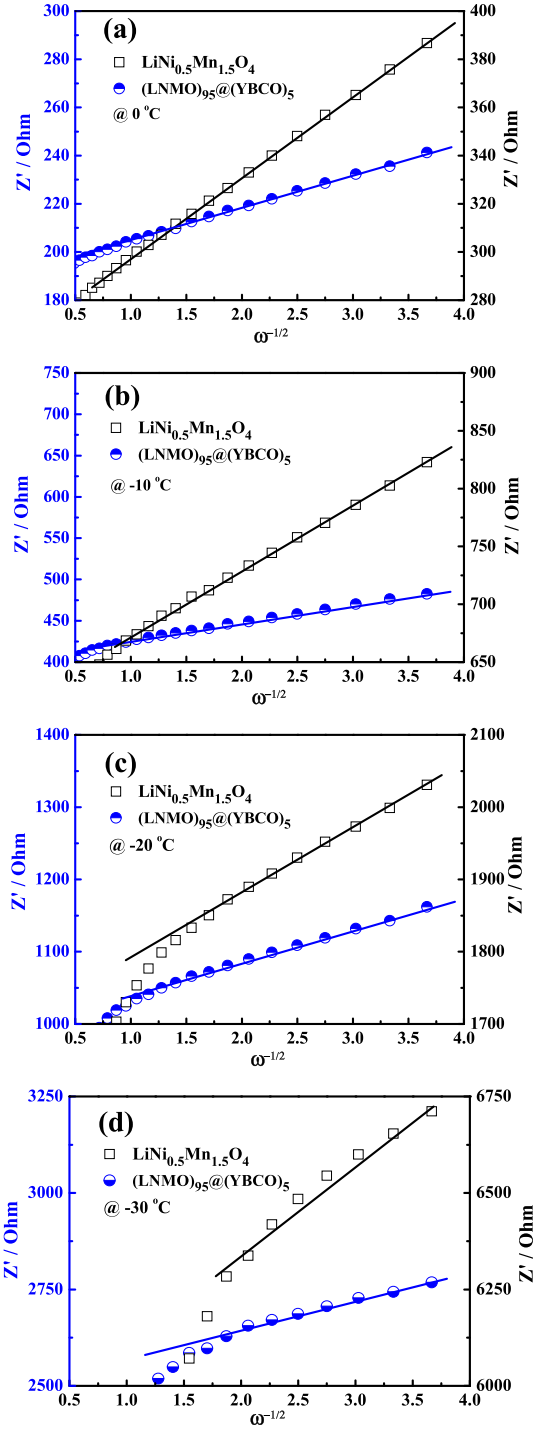

Fig. 11. Z' vs. $\omega^{-1/2}$ plots in the low frequency of $LiNi_{0.5}Mn_{1.5}O_4$ and $(LNMO)_{95}$@$(YBCO)_5$ at different temperature.

The chemical diffusion coefficient of Li^+ (D_{Li}^+) could be calculated according to the following equation [25]:

$$D_{Li}^{+} = \left(\frac{2RT}{\sqrt{2}n^2F^2\sigma_w AC}\right)^2 = \frac{2R^2T^2}{n^4F^4\sigma_w^2A^2C^2} \quad (1)$$

where R, T, A, F, n and C are the gas constant, the absolute temperature, the surface area of the electrode, the Faraday's constant, the number of electrons per molecule during oxidation, the Li^+ concentration in the cathode material, respectively. σ_w is the Warburg coefficient which has relationship with Z' as follows:

$$Z' = R_e + R_{ct} + \sigma_\omega \omega^{-1/2} \quad (2)$$

Fig. 11 represents the reciprocal square root of angular frequency ($\omega^{-1/2}$) dependence of the real impedance (Z') in the low frequency of $LiNi_{0.5}Mn_{1.5}O_4$ and $(LNMO)_{95}$@$(YBCO)_5$ at different temperature. Based on the linear plot slope of Z' *vs.* $\omega^{-1/2}$, it is found that lithium diffusion coefficient decreases with decreasing operation temperature, and the estimated diffusion coefficients of $(LNMO)_{95}$@$(YBCO)_5$ (0 °C: 4.456×10^{-10} cm^2 s^{-1}; −10 °C: 1.771×10^{-10} cm^2 s^{-1}; −20 °C: 3.779×10^{-11} cm^2 s^{-1}; −30 °C: 1.166×10^{-11} cm^2 s^{-1}) are higher than those of the pristine (0 °C: 7.404×10^{-11} cm^2 s^{-1}; −10 °C: 2.385×10^{-11} cm^2 s^{-1}; −20 °C: 9.285×10^{-12} cm^2 s^{-1}; −30 °C: 1.220×10^{-12} cm^2 s^{-1}) at the corresponding temperature. The obtained results further confirm that the enhancement on Li-ion diffusion at low temperature would be ascribed to the improved electrical wiring of the cathode particles by surface modification with high-conductive YBCO.

The superior electrochemical performances of $(LNMO)_{95}$ @$(YBCO)_5$ in a wide operation temperature could be explained by a

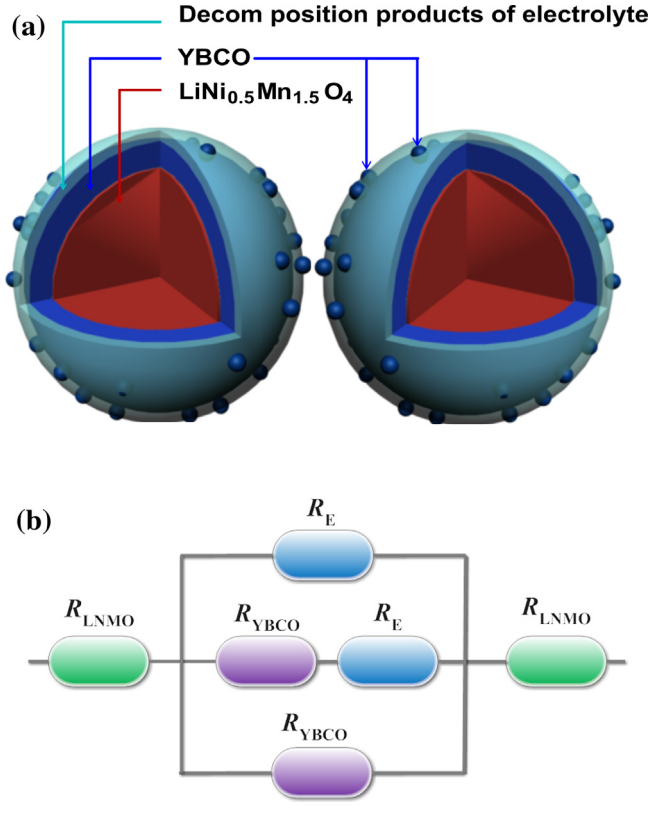

Fig. 12. (a) Schematic diagram of positive-electrode particle coated by YBCO and the species decomposition of electrolyte. (b) A phenomenological resistance model among $LiNi_{0.5}Mn_{1.5}O_4$ particles.

phenomenological resistance model based on scattering theory of electron transport across the interface [26]. Fig. 12 shows the corresponding equivalent electrical circuit between $LiNi_{0.5}Mn_{1.5}O_4$ particles describing these processes (Fig. 11b), where R_{LNMO}, R_{YBCO} and R_E present $LiNi_{0.5}Mn_{1.5}O_4$ resistance, YBCO resistance and the surface resistance arising from the species on cathode surface, respectively. It is well-established that the capacity fade mainly results from the formation of poor electronic-conductivity species among cathode particles. Considering that YBCO exhibits high conductivity in a wide temperature range, the loss of electrical contact among cathode particles would be reduced with the presence of YBCO on cathode surface based on the parallel circuit model, in which the total resistance in parallel strongly depends on the low-resistivity YBCO especially at low operation temperature. In addition, the presence of YBCO on $LiNi_{0.5}Mn_{1.5}O_4$ particles is expected to protect the active material from undesirable side-reactions between the electrolyte and electrode and consequently decrease the SEI and charge-transfer resistances. As a result, the cycling stability is improved with YBCO-coating, especially at elevated temperature.

4. Conclusions

Spinel $LiNi_{0.5}Mn_{1.5}O_4$ powders are coated with high-conductivity YBCO by a simple sol–gel process. Compared to the pristine $LiNi_{0.5}Mn_{1.5}O_4$, $(LNMO)_{95}@(YBCO)_5$ exhibits superior electrochemical performances in a wide operation temperature range. The obtained results reveal that the presence of superconducting YBCO on $LiNi_{0.5}Mn_{1.5}O_4$ surface plays an important role in decreasing the interfacial impedance, enhancing lithium diffusion rate especially at low temperature and suppressing the dissolution of transition metals from active materials in the $LiPF_6$ based electrolyte.

Acknowledgments

This work was supported by a grant from Natural Science Foundation of Fujian Province (No. 2013J01007) and Natural Science Foundation of China (No. 11344008), National Key Project for Basic Research of China under Grant No. 2011CBA00200.

References

[1] Q.M. Zhong, A. Bonakdarpour, M.J. Zhang, Y. Gao, J.R. Dahn, J. Electrochem. Soc. 144 (1997) 205.
[2] T. Ohzuku, S. Takeda, M. Iwanaga, J. Power Sources 81–82 (1999) 90.
[3] M. Kunduraci, J.F. Al-Sharab, G.G. Amatucci, Chem. Mater. 18 (2006) 3585.
[4] R. Santhanam, B. Rambabu, J. Power Sources 195 (2010) 5442.
[5] Y.C. Jin, C.Y. Lin, J.G. Duh, Electrochim. Acta 69 (2012) 45.
[6] G.Y. Zhao, Y.B. Lin, T. Zhou, Y. Lin, Y.D. Huang, Z.G. Huang, J. Power Sources 215 (2012) 63.
[7] H.W. Lee, P. Muralidharan, C.M. Mari, R. Ruffo, D.K. Kim, J. Power Sources 215 (2011) 10712.
[8] H.M. Wu, I. Belharouak, A. Abouimrane, Y.-K. Sun, K. Amine, J. Power Sources 195 (2010) 2909.
[9] D. Liu, J. Trottier, P. Charest, J. Fréchette, A. Guerfi, A. Mauger, C.M. Julien, K. Zaghib, J. Power Sources 204 (2012) 127.
[10] J.Y. Shi, C.–W. Yi, K. Kim, J. Power Sources 195 (2012) 6860.
[11] D.L. Liu, Y. Bai, S. Zhao, W.F. Zhang, J. Power Sources 219 (2012) 333.
[12] Y.K. Fan, J.M. Wang, Z. Tang, W.C. He, J.Q. Zhang, Electrochim. Acta 52 (2007) 3870.
[13] G. Krabbes, G. Fuchs, W.-R. Canders, H. May, R. Palka, High Temperature Superconductor Bulk Materials: Fundamentals - Processing - Properties Control - Application Aspects, Wiley-VCH, 2006.
[14] M. Kakihana, L. Borjesson, S. Eriksson, P. Svedlindh, J. Appl. Phys. 69 (1991) 867.
[15] M.S.M. Suan, M.R. Johan, Phys. C. 492 (2013) 49.
[16] F.Q. Cheng, Y.L. Xin, Y.Y. Huang, J.T. Chen, H.H. Zhou, X.X. Zhang, J. Power Source 239 (2013) 181.
[17] W.J. Zhang, J. Power Sources 196 (2011) 2962.
[18] K. Xu, Chem. Rev. 104 (2004) 4303.
[19] B.J. Hwanga, Y.W. Wu, M. Venkateswarlu, M.Y. Cheng, R. Santhanam, J. Power Sources 193 (2009) 828.
[20] J. Mao, K.H. Dai, Y.C. Zhai, Electrochim. Acta 63 (2012) 381.
[21] Y.-K. Sun, S.-T. Myung, B.-C. Park, H. Yashiro, J. Electrochem. Soc. 155 (2008) A750.
[22] H.B. Kang, S.T. Myung, K. Amine, S.M. Lee, Y.K. Sun, J. Power Source 196 (2010) 2023.
[23] M.Y. Mo, C.C. Ye, K. Lai, Z.Z. Huang, L.C. Zhu, G.Z. Ma, H.Y. Chen, K.S. Hui, Appl. Surf. Sci. 276 (2013) 635.
[24] Charl J. Jafta, Mkhulu K. Mathe, Ncholu Manyala, Wiets D. Roos, Kenneth I. Ozoemena, ACS Appl. Mater. Interfaces 5 (2013) 7592.
[25] J. Lin, D.B. Mu, Y. Jin, B.R. Wu, Y.F. Ma, Wu Feng, J. Power Source 230 (2013) 76.
[26] Z.G. Huang, Z.G. Chen, K. Peng, F.M. Zhang, Y.W. Du, Phys. Rev. B 69 (2004) 094420.